



**Michigan  
Technological  
University**

Michigan Technological University  
**Digital Commons @ Michigan Tech**

---

Data Science Publications

Data Science

---

2-18-2014

## Dynamical instability and Fermi surface topology in Ni<sub>2</sub>FeGa from first principles

Satyananda Chabungbam

*Institute of Advanced Study in Science and Technology, Gauhati University*

Gowtham S

*Michigan Technological University*

Munima Sahariah

*Institute of Advanced Study in Science and Technology*

Follow this and additional works at: <https://digitalcommons.mtu.edu/data-science-fp>

 Part of the [Engineering Commons](#)


---

### Recommended Citation

Chabungbam, S., S, G., & Sahariah, M. (2014). Dynamical instability and Fermi surface topology in Ni<sub>2</sub>FeGa from first principles. *Physical Review B*, 89(8), 085114-1-085114-6. <http://dx.doi.org/10.1103/PhysRevB.89.085114>

Retrieved from: <https://digitalcommons.mtu.edu/data-science-fp/10>

Follow this and additional works at: <https://digitalcommons.mtu.edu/data-science-fp>

 Part of the [Engineering Commons](#)

**Dynamical instability and Fermi surface topology in Ni<sub>2</sub>FeGa from first principles**Satyananda Chabungbam,<sup>1,2,\*</sup> S. Gowtham,<sup>3</sup> and Munima B. Sahariah<sup>1,\*</sup><sup>1</sup>*Institute of Advanced Study in Science and Technology, Guwahati 781035, India*<sup>2</sup>*Guwahati University, Guwahati 781014, India*<sup>3</sup>*Michigan Technological University, Houghton, Michigan 49931-1295, USA*

(Received 11 October 2013; revised manuscript received 23 December 2013; published 18 February 2014)

The phonon spectrum of stoichiometric Heusler alloy Ni<sub>2</sub>FeGa is calculated for the high-temperature cubic austenite phase by using first-principles density functional perturbation theory. We also compute the elastic constants of the alloy from the initial slopes of the acoustic phonon branch. The TA<sub>2</sub> phonon branch along [110] direction shows softening with a minimum dip at  $\zeta = 0.58$  which indicates the possibility of modulated phases prior to martensitic transformation. We also map the Fermi surface of this alloy both in 3D and 2D to check the presence of any nesting vectors. The observed nesting parameter is in good agreement with the above value of the wave vector in the [110] direction where phonon softening occurs.

DOI: [10.1103/PhysRevB.89.085114](https://doi.org/10.1103/PhysRevB.89.085114)

PACS number(s): 71.20.Lp, 63.20.dk, 81.30.Kf, 71.18.+y

**I. INTRODUCTION**

Shape memory alloys (SMAs) are considered as materials of technological importance for their shape memory effect and recoverable strain. One of the most widely used SMAs is nitinol. However, a more efficient class of SMAs known as ferromagnetic SMAs has received tremendous attention from researchers across the globe in the last few years. The speciality of these alloys lies in the fact that the shape memory can be driven by applying magnetic field which makes it possible to induce and recover strain cycles easily. Of these alloys, Ni<sub>2</sub>MnGa is the most studied Heusler alloy [1–6]. But its near stoichiometric composition shows brittleness, lower martensitic transformation temperature, and Curie temperature,  $T_c$ . In this context, Ni<sub>2</sub>FeGa has been reported to be a better alloy with better characteristics. It has a Curie temperature of 439 K and a martensitic phase transition temperature of 142 K in stoichiometric composition [7] and a higher 277 K in some off-stoichiometric compositions [8,9]. It has a two-way shape memory effect and shows a lower martensite saturation field of 0.6 T as compared to 1.0 T in the case of Ni<sub>2</sub>MnGa [7]. It has other interesting properties such as low transformation stress, high reversible strain, and small hysteresis [10]. The recoverable strain for this alloy is as high as 12% in the tetragonal L1<sub>0</sub> transformation [8]. The ductility of this alloy can be improved by the introduction of a small amount of the gamma phase [11]. Ni<sub>2</sub>FeGa has a comparatively higher linear dependence of transition temperature on the valence electron concentration than Ni<sub>2</sub>MnGa [12]. This indicates that the transition temperature in Ni<sub>2</sub>FeGa alloy can be easily controlled by a slight variation in its composition. Ni<sub>2</sub>FeGa exhibits first-order structural transformation from high-symmetry cubic austenite structure to low-symmetry tetragonal martensite structure on cooling and vice versa [13,14]. Many martensitic phases such as the modulated 5M, 6M, 7M, 10M, 14M phases are associated with such a transformation [8,11,15]. This means that some electronic and

structural precursor phenomena occur during the process of cooling before martensitic transformation. The microscopic origin of the martensitic transition has been correlated with acoustic phonon anomaly, Fermi nesting, and electron-phonon coupling in other similar alloys [6,16,17]. Pérez-Landazábal *et al.* found experimentally by inelastic neutron scattering that the TA<sub>2</sub> branch along [110] direction of the nonstoichiometric L2<sub>1</sub> phase of Ni<sub>2</sub>FeGa shows a slight softening around  $\zeta = 0.35$ . Moreover, elastic neutron scattering along the  $[\zeta\zeta 0]$  direction near (422) reflection shows a satellite peak close to  $\zeta = 0.33$  whose intensity decreases with cooling [18]. But not much theoretical work has been done regarding the microscopic origin of the dynamical instabilities in this system.

In our previous work [19], the structural, electronic, elastic, and magnetic properties of stoichiometric Ni<sub>2</sub>FeGa alloy were studied using first-principles calculation. In DOS calculation, a comparatively high electron density was observed just above and below the Fermi level suggesting that there might be some interesting electronic behavior near the Fermi level. This incites us to map the Fermi surface of stoichiometric Ni<sub>2</sub>FeGa Heusler alloy. The aim of this work is to give an explanation of the microscopic origin of the instabilities in stoichiometric Ni<sub>2</sub>FeGa alloy and consequently to check whether there is any relationship between phonon anomaly and Fermi nesting parameters.

**II. COMPUTATIONAL DETAILS**

In this work, we use DFT formalism [20,21] to calculate the electronic structure as well as the dynamical properties. All the calculations are done using the QUANTUM ESPRESSO package [22,23]. The Perdew-Burke-Ernzerhof (PBE) functionals [24] that come under the generalized gradient approximation (GGA) are used to address exchange-correlation interaction. To account for the interaction between the ionic cores and valence electrons, ultrasoft pseudopotentials are taken for Ni(3d<sup>8</sup>4s<sup>2</sup>), Fe(3d<sup>7</sup>4s<sup>1</sup>), and Ga(4s<sup>2</sup>4p<sup>1</sup>). For total energy calculation, the optimized plane wave kinetic energy cutoff is fixed at 40 Ryd and the density cutoff for ultrasoft pseudopotentials is fixed at 480 Ryd. The Methfessel-Paxton smearing technique for Brillouin zone integration has been employed

\*Authors to whom correspondence should be addressed: csatya11@gmail.com; munima@iasst.gov.in

for this metallic system. A smearing parameter of magnitude  $\sigma = 0.01$  Ryd is found to be appropriate for the desired results. All structural and electronic parameters are well converged over a  $k$ -mesh value of  $12 \times 12 \times 12$  Monkhorst-Pack grid. For vibrational studies, the density functional perturbation theory (DFPT) implemented in QUANTUM ESPRESSO is used to calculate the frequencies. The phonon energy convergence threshold is fixed at  $10^{-18}$  Ryd. The calculation of the phonon spectrum has been carried out over a  $q$  mesh of  $6 \times 6 \times 6$  Monkhorst-Pack which gives 16  $q$  points. The interatomic force constants are calculated by Fourier transformation of the dynamical matrices generated at each of the  $q$  points and finally interpolated back to get the full phonon dispersion spectra. For Fermi surface calculation, a uniform grid of  $12 \times 12 \times 12$  is used for scf calculation and a higher grid of  $28 \times 28 \times 28$  is used for nscf calculation. The bands that cross the Fermi level are identified using XCrySDen [25]. The 3D Fermi surface and 2D Fermi surface cross sections are generated from these bands.

### III. RESULTS AND DISCUSSION

$\text{Ni}_2\text{FeGa}$  is a full Heusler alloy that exists in at least two different stable phases, one in high-temperature cubic phase known as the austenite phase, the other in the low-temperature tetragonal phase known as the martensite phase. Of these two phases, the former is extensively studied in this work, which consequently provides useful information regarding the microscopic origin of the structural instabilities associated with this ferromagnetic alloy. In its austenite phase,  $\text{Ni}_2\text{FeGa}$  takes up the  $L2_1$  structure with space group  $Fm\bar{3}m$ . The two Ni atoms sit on the Wyckoff crystallographic positions  $(1/4, 1/4, 1/4)$  and  $(3/4, 3/4, 3/4)$ , while the Fe atom and Ga atom occupy the positions  $(1/2, 1/2, 1/2)$  and  $(0, 0, 0)$ , respectively. The austenite structure of  $\text{Ni}_2\text{FeGa}$  is shown in Fig. 1. The lattice constant of ferromagnetic  $\text{Ni}_2\text{FeGa}$  alloy in the  $L2_1$  structure is optimized by calculating the change in total energy as a function of lattice parameter.

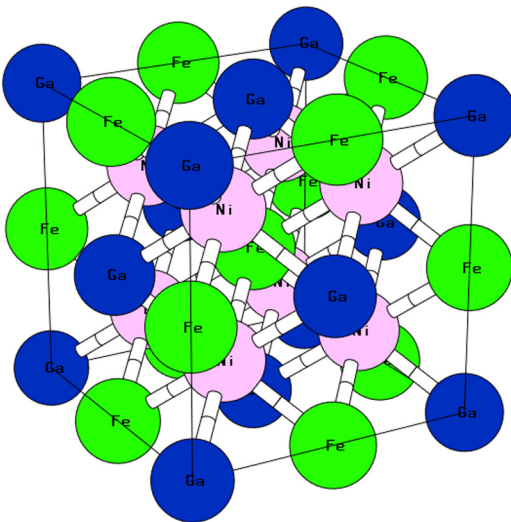


FIG. 1. (Color online)  $L2_1$  structure of stoichiometric  $\text{Ni}_2\text{FeGa}$  alloy.

TABLE I. Comparison of our optimized lattice constant and bulk modulus of  $L2_1$   $\text{Ni}_2\text{FeGa}$  with previous available theoretical and experimental data.

	$a$ (Å)	$B$ (GPa)
Experimental values	5.76 <sup>a</sup> 5.74 <sup>b</sup>	
Theoretical values	5.75 <sup>c</sup>	164 <sup>c</sup>
Our calculation	5.77	164.70

<sup>a</sup>Electron backscatter diffraction (EBSD) [26].

<sup>b</sup>X-ray diffraction (XRD) [7].

<sup>c</sup>*Ab initio* calculation by Bai *et al.* [27].

A fourth-order Murnaghan equation of states is fitted to the calculated total energies to get the equilibrium lattice constant and zero pressure bulk modulus. The calculated lattice parameter  $a = 5.77$  Å giving primitive cell volume  $V_0 = 47.99$  Å<sup>3</sup> is in good agreement with the experimental values 5.76 Å and 5.70 Å [7,26] and theoretical value 5.75 Å [27]. The calculated zero-pressure bulk modulus 164.70 GPa is in very good agreement with the previous theoretical value of 164 GPa [27]. The calculated pressure derivative of bulk modulus  $B'$  is found to be 5.32. Table I shows the comparative values of all the available data regarding lattice parameter and bulk modulus of  $\text{Ni}_2\text{FeGa}$  alloy.

Figure 2 shows the convergence of  $k$ -mesh for different degauss values. This convergence check is vital for dynamical studies of unstable systems as the soft phonon branch is sensitive to the degauss value. For higher degauss values, our desired energy convergence of 1 meV is achieved faster. The smaller the degauss value, the larger is the  $k$  mesh required.

The phonon spectrum of stoichiometric  $\text{Ni}_2\text{FeGa}$  is computed for a  $q$  mesh of order  $6 \times 6 \times 6$  with a phonon threshold convergence of  $10^{-18}$  Ryd. We have observed that there is significant softening of the  $\text{TA}_2$  branch along  $[110]$  direction. Such an anomaly known as Kohn anomaly basically arises due to screening of the lattice vibration by the conduction electrons. This type of anomaly is often related to Fermi surface nesting and electron-phonon coupling. The unstable phonons are in general sensitive to the variation of degauss values. In Fig. 3,

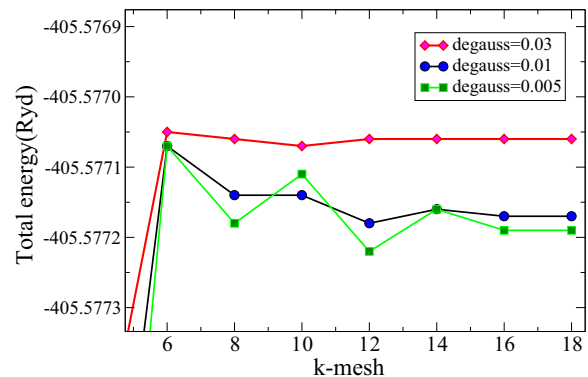


FIG. 2. (Color online)  $k$ -mesh convergence for different degauss values. The  $k$  mesh of the larger degauss value converges faster.

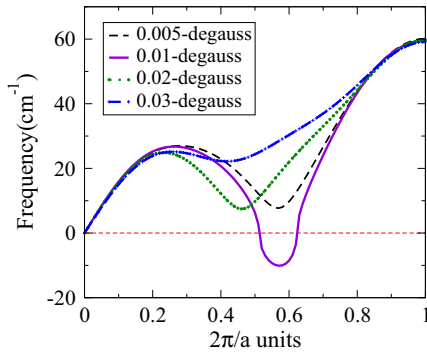


FIG. 3. (Color online)  $TA_2$  mode of  $Ni_2FeGa$  alloy along  $[110]$  direction at different degauss values showing convergence at  $\zeta = 0.58(110)$ .

the  $TA_2$  branches of phonon spectra along the  $[110]$  direction for different degauss values are shown explicitly. There are two factors as far as the convergence of the plots in Fig. 3 is concerned: first, convergence of frequency, and second, convergence of the wave vector for the phonon dip. It can be seen from the figure that the phonon dip has very well converged to wave vector  $\zeta = 0.58$  on lowering the degauss values. The contribution from the entropy part becomes less than 1 meV/atom [28] from  $\sigma = 0.01$  Ryd. The consistency and nontriviality of this result was checked by taking another  $q$  grid (444) and relaxing the phonon convergence threshold to  $10^{-16}$  Ryd. Calculations done with this set of parameters for  $\sigma = 0.03, 0.02, 0.01$  Ryd also gave the converged value of wave vector at  $\zeta = 0.58$  for the phonon dip. This result is in accordance with the result of Zayak and Entel [29], where they have shown the  $TA_2$  branches of six different magnetic Heusler alloys having structure of prototype  $Ni_2MnGa$ . According to them, the position of the softening of the branches changes with the change in valence electron concentration ( $e/a$ ). Their results show that the softening increases to larger value with increasing  $e/a$  value. Since the  $e/a$  value of  $Ni_2FeGa$  which is 7.75 is larger than that of  $Ni_2MnGa$  which is 7.5, it is expected that the premartensitic behavior shifts to larger wave vector in case of  $Ni_2FeGa$  than that of  $Ni_2MnGa$ . This is exactly what happens in our work where we observed the phonon softening wave vector to be  $\zeta = 0.58$  which is larger than  $\zeta = 0.33$  of  $Ni_2MnGa$  [6,30]. As for the phonon frequencies of the  $TA_2$  mode, they do not show any trend which of course would not hamper the qualitative understanding of the phenomena of dynamical instability in this particular alloy. The high sensitivity of the unstable modes to various input parameters might have given rise to some numerical instability which is causing fluctuation in the phonon frequency. The full phonon spectra for degauss values 0.01 Ryd and 0.005 Ryd are shown in Fig. 4. The figure shows that except the  $TA_2$  modes along  $[110]$  direction, almost all other branches both for acoustic and optical modes are overlapping. This is also reflected in the total phonon density of states presented sidewise in the same figure.

The significant softening of the  $TA_2$  mode along the  $[110]$  direction in the phonon spectra with a minimum dip at  $\zeta = 0.58$  as discussed above is indicative of the notion that a larger  $\zeta$  value corresponds to a higher modulated structure

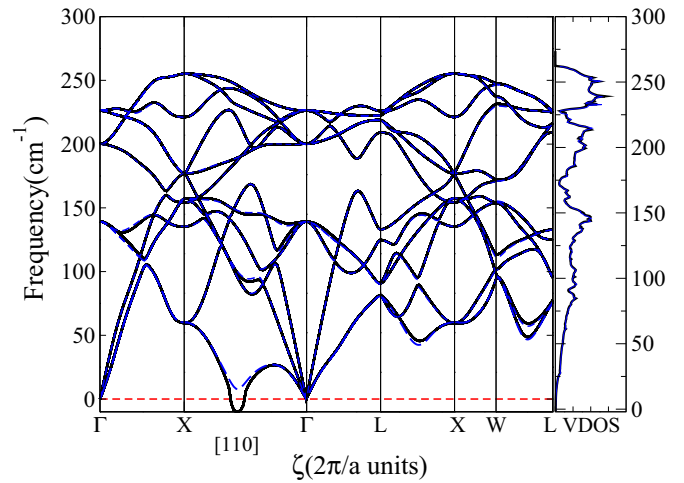


FIG. 4. (Color online) Phonon spectra of  $Ni_2FeGa$  alloy showing softening along  $[110]$  with a minimum dip at  $\zeta = 0.58(110)$ . The full (black) lines represent the spectrum for degauss 0.01 Ryd while the dashed (blue) lines represent the spectrum for degauss 0.005 Ryd.

like the 5M or 7M structures in the premartensite phase as predicted by Velikokhatny *et al.* in the case of  $Ni_2MnGa$  [16]. Since the degauss value is related to the electronic temperature, the sensitivity of the unstable acoustic mode indicates that there might be anharmonic interactions in the system. However Pérez-Landazábal *et al.*'s experimental neutron scattering result found this minimum dip at  $\zeta = 0.35$  [18]. The main discrepancy between our result and the experimental findings is mainly due to the fact that Pérez-Landazábal *et al.* performed the experiments at 300 K which is critically above the martensitic transformation temperature and used an off-stoichiometric sample  $Ni_{51.5}Fe_{21.5}Ga_{27.0}$  (at. %). In this regard, the sensitiveness of  $Ni_2FeGa$  over  $Ni_2MnGa$  in terms of composition may be noted [12]. Such discrepancy between experimental and theoretical results for phonon softening can also be observed in the case of  $Ni_2MnGa$  [5]. The acoustic phonon anomaly that appears in the full phonon spectra shows that the  $L2_1$  structure is not stable at low temperature which is expected. This also suggests that there might be some unstable phases with modulated structures prior to martensitic transformation [8,11]. In the case of  $Ni_2MnGa$  which also shows such a complete softening, the dip appears at  $\zeta = 0.33$  and consequently leads to the premartensitic modulated 3M superstructure [30].

Figure 5 shows the projected vibrational density of states of  $Ni_2FeGa$  along with the total density of states. Here the lower acoustic region and the first peak around  $145\text{ cm}^{-1}$  in the total DOS is mainly contributed by Ni atoms while the second peak around  $212\text{ cm}^{-1}$  has a main contribution from Fe atoms with some contributions from Ni and Ga atoms as well. Ga atoms have the maximum contribution to the highest optical peak in  $Ni_2FeGa$  whereas in the case of  $Ni_2MnGa$ , Mn atoms contribute more to the highest optical peak. Here it is interesting to see that the heaviest element Ga among the three is contributing most to the highest frequency peak which invites more investigation. As can be seen from Fig. 5, there is more or less uniform distribution of frequency across the

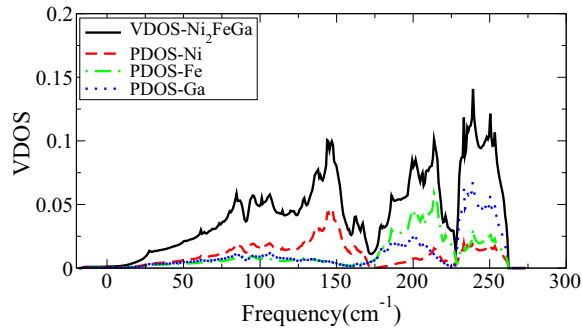


FIG. 5. (Color online) Partial vibrational density of states (DOS) of each atomic species plotted together with total vibrational DOS of  $\text{Ni}_2\text{FeGa}$ .

acoustic range as compared to the optical range where we find more distinct peaks.

We have calculated the elastic constants from the slopes of acoustic phonons in the long-wavelength limit which is a good test for the reliability of the phonon spectra. The elastic constants  $C_{44}$  and  $C'$  are evaluated from the  $\text{TA}_1$ ,  $\text{TA}_2$  branches along  $[110]$  while  $C_{11}$  is evaluated from the LA branch along the  $[100]$  direction. We have tabulated the calculated values of elastic constants along with the available previous theoretical and experimental values as shown in Table II. The calculated elastic constants are within acceptable range with the available previous data. The value of  $C_{44}$  is within 12.8 % of the experimental value whereas the values of  $C'$  and  $C_{11}$  are higher than the experimental ones. At this point, we should mention that there is only one experimental work giving elastic constants and that also not in the same composition as ours. Moreover, we find that such a discrepancy exists in the case of  $\text{Ni}_2\text{MnGa}$  also [31].

Since we are doing investigations in a metallic system, it is important to understand the Fermi surface topology. The magnetic and transport properties of the metallic systems are directly or indirectly related to the shape of the Fermi surface and the associated nesting vector. Previous studies on prototype ferromagnetic SMA  $\text{Ni}_2\text{MnGa}$  provides many elementary ideas regarding shape memory effect and phenomena associated with this type of alloy from the Fermi surface. In  $\text{Ni}_2\text{MnGa}$ , Shapiro *et al.*'s observation of a 3D charge-density-wave phase through phasons in the M phase was believed to be related to Fermi surface nesting [32]. Bungaro *et al.* found that  $\text{Ni}_2\text{MnGa}$  shows phonon anomaly along the  $[110]$  direction and tried to find the nesting vectors in

TABLE II. Elastic constants calculated from initial phonon slopes compared with previous experimental and theoretical values.

	$C_{44}$	$C'$ ( $10^{12}$ dyns/cm $^2$ )	$C_{11}$
Experimental	0.86 <sup>a</sup>	0.13 <sup>a</sup>	1.63 <sup>a</sup>
Theoretical	1.04 <sup>b</sup>	-0.02 <sup>b</sup>	1.62 <sup>b</sup>
Our calculation	0.75	0.32	2.23

<sup>a</sup>Phonon dispersion by inelastic neutron scattering experiments [18].

<sup>b</sup>Lattice deformation by GGA-DFT *ab initio* theory [19].

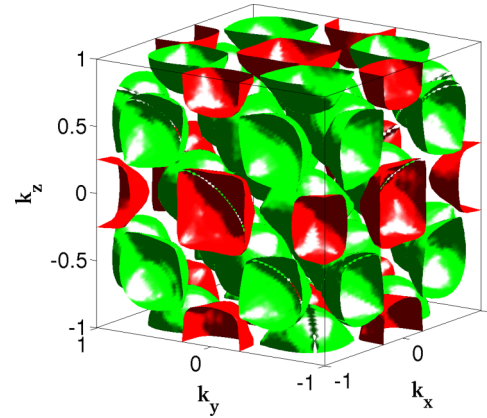


FIG. 6. (Color online) 3D Fermi surface topology of  $\text{Ni}_2\text{FeGa}$  alloy. The Fermi surfaces that occupy the center of each face and edge (red) are the 20th bands of minority spin bands while the other Fermi surfaces in between (green) represent the 19th bands of minority spin bands.

this alloy [6]. Velikokhatnyi and Naumov [16] calculated the generalized susceptibility for the  $\text{Ni}_2\text{MnGa}$  system and found two significant peaks corresponding to two nesting vectors in the Fermi surface suggesting that these two nesting parameters might be responsible for the 5M and 7M modulated structures in the system. Lee *et al.*'s [17] calculations on  $\text{Ni}_2\text{MnGa}$  by using the scalar relativistic LMTO method reported that the nesting feature evolves with the variation in magnetization.

But Haynes *et al.*'s [33] recent experimental investigations on  $\text{Ni}_2\text{MnGa}$  reported that the reconstructed Fermi surface shows a nesting vector at  $\mathbf{q} = [0.47, 0.47, 0]$ . This vector is said to be very close to nearly tetragonal 5M modulating vector below  $T_m$ . The above findings strongly suggest that various modulated structures in the premartensite phase of ferromagnetic Heusler alloys are associated with Fermi surface nesting, generalized susceptibility peaks, and phonon anomalies. But it cannot be generalized that all ferromagnetic Heusler alloys show all the above-mentioned features.  $\text{Co}_2\text{NiGa}$  is one exception which shows neither phonon anomaly nor Fermi surface nesting [34]. Our main aim here is to check any correlation between phonon anomalies and Fermi surface nesting in  $\text{Ni}_2\text{FeGa}$ .

The three-dimensional Fermi surface topology for stoichiometric  $\text{Ni}_2\text{FeGa}$  is shown in Fig. 6. Here we concentrate only on the minority spin states as it was observed in our previous calculations on electronic structure that the minority spin states took a major part in stabilizing the martensitic phase [19]. The 19th band and 20th band of the minority spin states are presented in this 3D plot. The flat portions of the Fermi surfaces of both the minority spin bands are very obvious at the zone boundary. But our focus area is whether this flatness continues to other parts of the Brillouin zone or not. To probe this idea, we cut the 3D Fermi surface at different  $K_z$  planes. Figure 7 shows the 2D cross sections of the Fermi surface of two  $K_z$  planes. Here, we considered only the interband nesting between the 19th and 20th band of the minority spin states. The blue dotted lines indicate the cross section at  $K_z = 1.00$  while the solid red lines indicate the cross section at  $K_z = 0.95$ . We see that the two lines almost overlap in most areas signifying

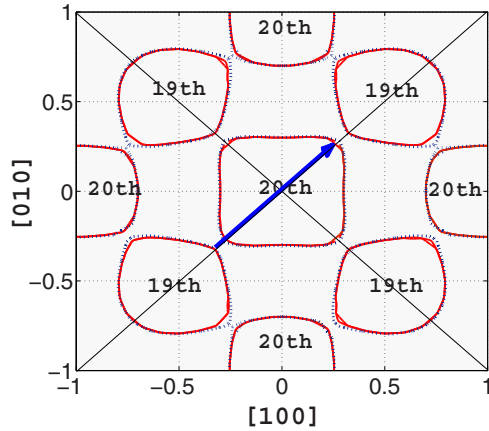


FIG. 7. (Color online) 2D cross section of Fermi surface of  $\text{Ni}_2\text{FeGa}$  along  $k_z = 1.0$  (dotted lines) and  $k_z = 0.95$  (solid lines) planes showing Fermi nesting vector  $\mathbf{q} = 0.58(110)$  represented by the arrow (blue) extending from the 19th band to the 20th band.

that the flat portions of the Fermi surface are extended to a reasonable extent in the whole Brillouin zone. The arrow at the center extending from the 19th band to the 20th band represents the observed nesting vector  $\mathbf{q} = 0.58$  along the  $[110]$  direction. The observed Fermi surface nesting might enhance the effect of electron-phonon coupling in this alloy. There is enough scope of experimental works in this case for calculating the generalized susceptibility which would help us to further visualize the observed nesting vectors with the peaks in the susceptibility spectrum. The nesting vector that we observed from Fermi surface calculations exactly matches the wave vector of the  $\text{TA}_2$  phonon dip calculated along the  $[110]$  direction.

#### IV. CONCLUSIONS

The observed phonon anomaly in the  $\text{TA}_2$  branch along  $[110]$  shows the instability of the cubic  $\text{Ni}_2\text{FeGa}$  system at the calculated temperature 0 K. The complete softening of this branch with a minimum dip at  $\zeta = 0.58(110)$  might be responsible for the occurrence of various intermediate modulated superstructures 5M, 6M, 7M, 10M observed experimentally. Another remarkable feature of the  $\text{TA}_2$  phonon branch is that it is found to be sensitive with respect to degauss value. This phonon branch shows remarkable change in the magnitude of softening and position of the minimum dip with the variation of degauss values. We observed interband Fermi surface nesting behavior in the down-spin states of the 19th and 20th bands. The observed Fermi surface nesting vector  $\mathbf{q} = 0.58(110)$  exactly matches the soft phonon wave vector in the full phonon spectra. This confirms that the two microscopic parameters, i.e., the Fermi nesting vectors and acoustic phonon anomaly, are well connected and might play a major role in destabilizing premartensitic phenomena. There is a strong belief that this higher value of wave vector  $\mathbf{q} = 0.58(110)$  may be a signature of the presence of higher modulated structures such as the 5M or 7M in the premartensite phase of this alloy. Further investigations on modulated superstructures in stoichiometric and off-stoichiometric compositions may give a better insight in understanding this smart alloy.

#### ACKNOWLEDGMENTS

S.C. and M.B.S. would like to acknowledge the Department of Physics, Michigan Technological University, USA, for providing HPC facilities, and the help of Prof. Derek Stewart, Cornell University, USA, in plotting the Fermi surface. M.B.S. would also like to acknowledge support from DST, Government of India, through Project No. SR/FTP/PS-031/2012.

- 
- [1] M. E. Gruner, W. A. Adeagbo, A. T. Zayak, A. Hucht, S. Buschmann, and P. Entel, *Eur. Phys. J. Spec. Top.* **158**, 193 (2008).
- [2] V. D. Buchelnikov, V. V. Sokolovskiy, S. V. Taskaev, V. V. Khovaylo, A. A. Aliev, L. N. Khanov, A. B. Batdalov, P. Entel, H. Miki, and T. Takagi, *J. Phys. D: Appl. Phys.* **44**, 064012 (2011).
- [3] S. Ghosh, L. Vitos, and B. Sanyal, *Physica B* **406**, 2240 (2011).
- [4] Q. M. Hu, C. M. Li, R. Yang, S. E. Kulkova, D. I. Bazhanov, B. Johansson, and L. Vitos, *Phys. Rev. B* **79**, 144112 (2009).
- [5] M. A. Uijtewaal, T. Hickel, J. Neugebauer, M. E. Gruner, and P. Entel, *Phys. Rev. Lett.* **102**, 035702 (2009).
- [6] Claudia Bungaro, K. M. Rabe, and A. Dal Corso, *Phys. Rev. B* **68**, 134104 (2003).
- [7] Z. H. Liu, M. Zhang, Y. T. Cui, Y. Q. Zhou, W. H. Wang, G. H. Wu, X. X. Zhang, and G. Xiao, *Appl. Phys. Lett.* **82**, 424 (2003).
- [8] R. F. Hamilton, C. Efstathiou, H. Sehitoglu, and Y. Chumlyakov, *Scr. Mater.* **54**, 465 (2006).
- [9] D. Pal and K. Mandal, *J. Phys. D: Appl. Phys.* **43**, 455002 (2010).
- [10] H. Sehitoglu, J. Wang, and H. J. Maier, *Int. J. Plasticity* **39**, 61 (2012).
- [11] K. Oikawa, T. Ota, T. Ohmori, Y. Tanaka, H. Morito, A. Fujita, R. Kainuma, K. Fukamichi, and K. Ishida, *Appl. Phys. Lett.* **81**, 5201 (2002).
- [12] Z. H. Liu, H. Liu, X. X. Zhang, M. Zhang, X. F. Dai, H. N. Hu, J. L. Chen, and G. H. Wu, *Phys. Lett. A* **329**, 214 (2004).
- [13] E. Alvarado-Hernandez, D. E. Soto-Parra, R. Ochoa-Gamboa, P. O. Castillo-Villa, H. Flores-Zuniga, and D. Rios-Jara, *J. Alloys Compd.* **462**, 442 (2008).
- [14] Y. Li, C. Jiang, T. Liang, Y. Ma, and H. Xu, *Scr. Mater.* **48**, 1255 (2003).
- [15] H. R. Zhang, C. Ma, H. F. Tian, G. H. Wu, and J. Q. Li, *Phys. Rev. B* **77**, 214106 (2008).
- [16] O. I. Velikokhatny and I. I. Naumov, *Phys. Solid State* **41**, 4 (1999).
- [17] Y. Lee, J. Y. Rhee, and B. N. Harmon, *Phys. Rev. B* **66**, 054424 (2002).
- [18] J. I. Pérez-Landazábal, V. Recarte, V. Sanchez-Alarcos, J. A. Rodriguez-Velamazan, M. Jimenez-Ruiz, P. Link, E. Cesari, and Y. I. Chumlyakov, *Phys. Rev. B* **80**, 144301 (2009).
- [19] M. B. Sahariah, S. Ghosh, C. S. Singh, S. Gowtham, and R. Pandey, *J. Phys.: Condens. Matter* **25**, 025502 (2013).
- [20] P. Hohenberg and W. Kohn, *Phys. Rev.* **136**, B864 (1964).

- [21] W. Kohn and L. J. Sham, *Phys. Rev.* **140**, A1133 (1965).
- [22] P. Giannozzi *et al.*, *J. Phys.: Condens. Matter* **21**, 395502 (2009); <http://www.quantum-espresso.org>
- [23] S. Scandolo, P. Giannozzi *et al.*, *Z. Kristallogr.* **220**, 574 (2005).
- [24] J. P. Perdew, K. Burke, and M. Ernzerhof, *Phys. Rev. Lett.* **77**, 3865 (1996).
- [25] A. Kokalj, *Comput. Mater. Sci.* **28**, 155 (2003).
- [26] Y. Sutou, N. Kamiya, T. Omori, R. Kainuma, K. Ishida, and K. Oikawa, *Appl. Phys. Lett.* **84**, 1275 (2004).
- [27] J. Bai, J. M. Raulot, Y. D. Zhang, C. Esling, X. Zhao, and L. Zuo, *J. Appl. Phys.* **109**, 014908 (2011).
- [28] G. Kresse and J. Furthmuller, *Comput. Mater. Sci.* **6**, 15 (1996).
- [29] A. T. Zayak and P. Entel, *J. Magn. Magn. Mater.* **290-291**, 874 (2005).
- [30] A. T. Zayak, P. Entel, J. Enkovaara, A. Ayuela, and R. M. Nieminen, *Phys. Rev. B* **68**, 132402 (2003).
- [31] Alexey T. Zayak, Ph.D. thesis, University of Duisburg, Germany, 2003.
- [32] S. M. Shapiro, P. Vorderwisch, K. Habicht, K. Hradil, and H. Schneider, *Europhys. Lett.* **77**, 56004 (2007).
- [33] T. D. Haynes, R. J. Watts, J. Laverock, Zs. Major, M. A. Alam, J. W. Taylor, J. A. Duffy, and S. B. Dugdale, *New J. Phys.* **14**, 035020 (2012).
- [34] M. Siewert, M. E. Gruner, A. Dannenberg, A. Hucht, S. M. Shapiro, G. Xu, D. L. Schlagel, T. A. Lograsso, and P. Entel, *Phys. Rev. B* **82**, 064420 (2010).